Second Harmonic Generation in 1D Nonlinear Plasma Photonic Crystals

Cheng Yang, Chu-Ming Guo, Chuan Peng, and Hai-Feng Zhang*

In this paper, a 1D nonlinear plasma photonic crystal (NPPC) structure composed of polarized ferroelectric crystals and nonlinear plasma periodic alternation is proposed. The transfer matrix method is employed to analyze the second harmonic generation (SHG) problem of this structure. In the designed NPPCs, the fundamental wave (FW) operates in the gigahertz (GHz) band and the nonlinear plasma is controlled by an external high-intensity control wave (CW). Numerical simulations are performed to investigate the effects of different incident angles and external CW intensities on the total conversion efficiency (T-con) of the second harmonic wave (SHW). Additionally, the internal electric field distribution and incident light intensity within the nonlinear structure are analyzed. The importance of the relationship between the FW frequency and photonic band gap (PBG) in enhancing SHG is summarized. The results demonstrate that the optimal structure can be obtained by changing the structural parameters, such that the FW and SHW are tuned to the edge of the PBG. At this point, the electromagnetic field density is large, the group velocity is small, the local field is enhanced, and the nonlinear optical interaction is increased, resulting in a significant increase in the T-con of the SHW.

1. Introduction

Photonics crystals (PCs)[1–3] have received extensive attention and research due to their unique photonic band gap (PBG) properties. The simplest PBG structure is the fiber Bragg grating,[4] which has been widely used in practical applications in optical communication systems. However, traditional PCs have the disadvantage of non-tunable PBG. Therefore, the plasma photonic crystals (PPCs)[5] can be proposed to address this issue. Plasmas, which primarily exhibit magnetic-optical effects, are influenced by external electromagnetic fields in nature.[6] In 2004, Japanese scholars Hojo and Mase[7] first proposed the concept of PPCs. The Drude model[8] of PPCs, which defines the structure of plasma and dielectric arranged periodically in space, can be used to describe uniform plasma in space, but it is difficult to achieve. If an external magnetic field is introduced into the plasma, it will exhibit strong diffusion[9] and dissipation.[10] Scholar Shiveshwari studied the PBG structure of 1D PPCs using the transmission matrix method and discussed the effects of plasma layer density, width, and period on the PBG structure,[11] demonstrating that it is easy to obtain tunable structures when plasma is introduced into PCs.

On the one hand, in recent years, significant progress has been made in the study of PCs in the field of nonlinear optics. The preparation and study of PPCs with periodic changes in nonlinear polarization have become a current research hotspot, and the use of nonlinear photonic crystals (NPCs)[12,13] to expand the field of optics and produce optical devices has become an important research direction. The existence of PBG enables the combination of nonlinear effects and PCs to generate many remarkable phenomena, such as PBG drift,[14] nonlinear induced self-trapping,[15] second harmonic generation (SHG),[16] difference frequency,[17] optical bistability,[18] and optical parametric oscillators.[19] Among them, SHG has received extensive research attention since it can effectively extend the laser bandwidth and obtain the required light source frequency. In 1995, Trull[20] et al. found that 1D NPCs structure with defects could enhance the excitation effect of SHG, and in 2004, Xu[21] et al. found that PCs grating structures could simultaneously generate second and third harmonic and achieve phase matching. Against the background of SHG, quasi-phase matching (QPM) technology[22,23] has been continuously developed and is considered an attractive method for obtaining good phase matching and improving second harmonic conversion efficiency. Compared with the usual perfect phase matching[24,25] (temperature matching, angle matching), QPM can more easily utilize larger nonlinear coefficients. In addition, periodically poled ferroelectric crystals (FCs) (LiNbO$_3$, LiTaO$_3$, KTiOPO$_4$) are widely used in the study of nonlinear optical interactions due to their spontaneous polarization.[26,29] Improving the nonlinear conversion efficiency is a long-term goal of periodically poled FCs.

On the other hand, in recent years, the hotspot of scientific research has mainly focused on the study of PBG in the PPCs and the influence of changing plasma parameters on PBG. However, the nonlinear studies of PPCs have not been explored. Research on the design of microwave devices using

C. Yang, C.-M. Guo, C. Peng, H.-F. Zhang
College of Electronic and Optical Engineering and the College of Flexible Electronics (Future Technology)
Nanjing University of Posts and Telecommunications (NJUPT)
Nanjing 210023, P. R. China
E-mail: hanlor@njupt.edu.cn

The ORCID identification number(s) for the author(s) of this article can be found under https://doi.org/10.1002/andp.202300190

ADVANCED
SCIENCE NEWS

www.advancedsciencenews.com
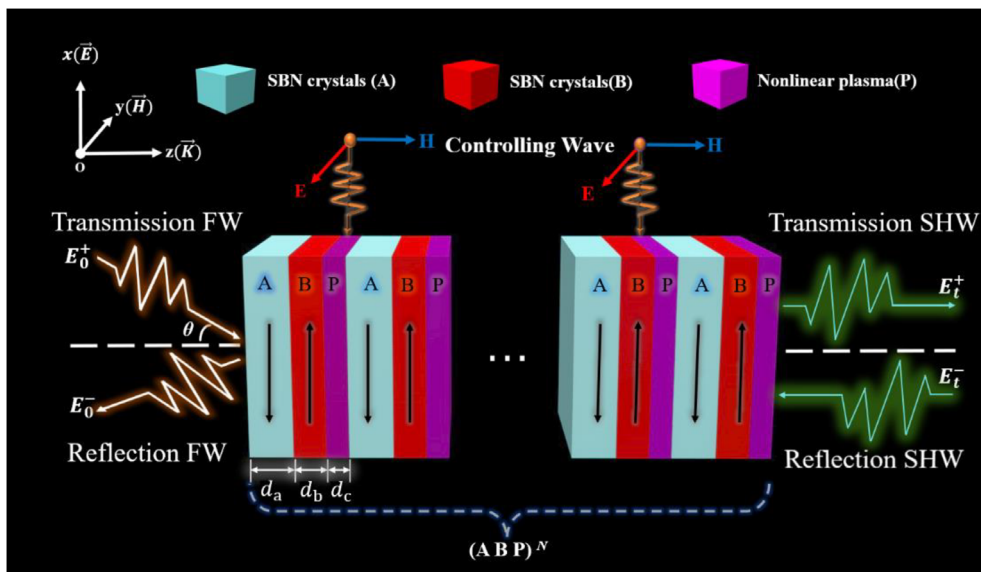
annalen
der **physik**

www.ann-phys.org

Figure 1. Schematic diagram of the proposed 1D NPPCs.

nonlinear plasma photonic crystals (NPPCs) is lacking. Nonlinear plasma (NP) and PCs composed of nonlinear materials with periodic or quasiperiodic arrangements have not received sufficient attention. Sakai,[31] a Japanese scholar, introduced nonlinear materials into the study of electromagnetic properties of metamaterial structures and summarized the band structure, negative refraction phenomenon, and nonlinear phenomena[32,33] of plasma metamaterials. He proposed the possibility of using plasma as a Kerr nonlinear material. By combining the various properties of NP with PCs, phenomena such as PBG shifts,[34] nonlinear-induced self-trapping,[15] high harmonic generation,[35] four-wave mixing,[36] and optical bistability[37] can be produced. In addition, by utilizing the nonlinear optical properties of plasma, the electromagnetic properties of NPPCs in the optical wave frequency range can be applied to the microwave field. Combining NP with nonlinear materials and studying their SHG in the microwave frequency range is a current and potentially important research direction.

Therefore, in this article, a novel 1D NPPCs structure is proposed, in which the NP layer is controlled by an external high-intensity control wave (CW), and the effect of changes in the amplitude of each layer on the parameters of the NP can be ignored. The FCs dielectric layer is composed of periodically polarized strontium barium niobate (SBN) crystals, with a second-order nonlinear coefficient $\chi^{(2)} = 27.2$ pmV^{-1}.[38] Furthermore, according to the nonlinear optics theory, the second-order nonlinear coefficient range of commonly used gas and solid plasma materials is between 10^{-4} to 10^{-5} esu.[39] It can be seen that the nonlinear coefficients of SBN and the NP are both very small. Hence, within the entirety of the structure, it is posited that the nonlinear process is comparatively weak, and as a result, the FW is essentially impervious to the influence of the nonlinear material. To ameliorate the intricacy of nonlinear optical quandaries in the medium, most conventional transfer matrix methods resort to approximations of a certain ilk, thereby falling short of complete accuracy. Nevertheless, the transfer matrix method uti-

lized in this study can more precisely grapple with the issue of SHG. This paper's architecture is arranged as follows: Section 2 is initiated by modulating the refractive index of the FCs and NP, succeeded by the derivation of the pertinent transmission matrix predicated on the designed 1D NPPCs structure. Furthermore, the SHG procedure is elucidated. In Section 3, the modulation effects of the nonlinear structure thickness, incident wave optical intensity, CW intensity, and angle parameters on the structure are studied. An optimized structure design is proposed based on the conditions of the high density of electromagnetic transmission modes and low velocity of electromagnetic waves near PBG. Furthermore, a constrained cavity is employed to achieve the optimal conversion efficiency of the second harmonic wave (SHW). Ultimately, the study's results are summarized, and conclusions are drawn.

2. Model Construction and Formulation

In this section, the multilayer nonlinear structure integrating FCs with NP is investigated, where both the linear and nonlinear optical characteristics are periodically modulated. The entire structure, as illustrated in **Figure 1**, is situated against an air background and incident at an angle of θ. In this structure, the scales of the linear and nonlinear parameters are the same. In addition, the 1D NPPCs structure is composed of two materials, namely periodically polarized SBN crystals (described by A and B) and the NP (described by P), filled with different colors. The arrangement of the entire structure can be represented as "(ABP)N." The thickness and nonlinear optical parameters of A are d_a, $n_a^{(m)}$ and $\chi^{(2)}$, respectively, and the length and nonlinear parameters of B are d_b, $n_b^{(m)}$ and $-\chi^{(2)}$, respectively. Here, m is either f or s, where f represents the FW field and s represents the SHW field. The length of the nonlinear plasma layer P is d_p, $n_p^{(m)}$ and $\chi_p^{(2)}$. Due to the refractive index mismatch between the three-layer interfaces, reflections occur at each layer interface, leading to interference

**ADVANCED
SCIENCE NEWS**

www.advancedsciencenews.com

annalen
der **physik**

www.ann-phys.org

between the transmitted and reflected waves in each layer.[40] In Figure 1, it is assumed that an electromagnetic wave with frequency and incident angle enters the system from the left and propagates along the z-axis. The periodic polarization direction of the FCs in layers A and B are along the x-axis. The numerical calculation method for the propagation of the FW in the 1D NPPCs structure is based on the nonlinear transfer matrix method. The entire SHG process is divided into four stages: (1) First, the refractive indices of the SBN layers and NP layer are modulated separately; (2) then, the FW field causes macroscopic polarization in the material as it propagates through the structure; (3) due to the nonlinearities of the FCs material and plasma material, second-order nonlinear polarization is generated in the material, leading to the radiation of the SHW field in the structure; (4) this SHW field propagates throughout the entire structure and is output in the form of a second harmonic signal.

First, the modulation of the refractive index in a three-layer structure was discussed. For the FCs (A and B) layers, we use SBN to generate nonlinear effects. SBN, as a type of niobate crystals, has a high optical nonlinear coefficient and low dispersion, making it widely used in optical communication and laser fields. Particularly in the laser field, SBN can be used to produce SHW and difference frequency and other nonlinear optical processes.[41] In this paper, we utilize the nonlinear effect of SBN crystal to generate the SHW, and control it through the NP (medium P). When the FW propagate in the SBN crystal, it will cause the optical path difference, which in turn affects the efficiency of SHG by modulating the refractive index. When an electric field is applied along the z-axis to the SBN crystal for electro-optic modulation, the refractive index of the SBN layer can be expressed as follows:[42]

$$n_a = n_0 + \Delta n_a = n_0 - \frac{1}{2}n_0^3 r_{33} E \tag{1}$$

Here, r_{33} represents the electro-optic coefficient, E is the electric field amplitude, and the refractive index n_0 is represented as follows:[42]

$$n_0^2 = O + \frac{U}{\lambda^2 - V^2} - W\lambda^2 \tag{2}$$

In this context, $O = 5.065$; $U = 11.13 \times 10^4$; $V = 6.7525 \times 10^4$; $W = 1.605 \times 10^{-5}$. The optical–electric coefficients of the material in different layers have different signals, which are the same as the nonlinear optical coefficients. As shown in Figure 1, the black arrow represents the polarization direction of the FCs. In the reverse B-layer, the optical-electric coefficients and the corresponding modulated refractive index can be expressed as follows:

$$n_b = n_0 + \Delta n_b = n_0 + \frac{1}{2}n_0^3 r_{33} E \tag{3}$$

The electro–optic modulation of SBN is based on the Kerr effect. Under the action of an external electric field, the refractive index of the crystal undergoes a slight change, which is proportional to the magnitude of the electric field. Therefore, by controlling the magnitude of the external electric field, the refractive index can be changed, thereby changing the propagation speed and phase of the pump wave through the structure, and achiev-

ing the control of the optical signal. Ultimately, the PBG becomes accessible in the FCs layer.

Let us discuss the refractive index modulation of the P layer. The NP is assumed to be non-magnetized and satisfies the Kerr nonlinear condition. For materials with the nonlinear Kerr effect, the dielectric constant ε can be expressed as:[33]

$$\varepsilon = \varepsilon^L + \varepsilon^{NL} = \varepsilon^L + \varepsilon_0 \langle \chi \rangle E^2 \tag{4}$$

In Equation (4), L represents the linear part, NL and $\langle \chi \rangle$ represent the nonlinear and polarization parts, respectively. Combining with the continuous equation of particle transport:[33]

$$\frac{\partial n_e}{\partial t} + \nabla \cdot (\eta_e n_e E - F \cdot \nabla n_e) = n_e v_{de} \alpha(E, P) - L_e \tag{5}$$

Here, the electron mobility and electron diffusion coefficient are η_e and F, respectively. α and L_e respectively denote the ionization coefficient and electron loss rate. By using Equation (5), the dielectric constant ε_p of the NP can be expressed as:[33]

$$\varepsilon_p = 1 - \frac{e^2 \eta_e}{\varepsilon_0 m_e \beta \omega^2 (1 + j v_m / \omega)} \cdot E \cdot \alpha(EP) \tag{6}$$

During the incident process, the electric field amplitude generated by the FW is different in each layer of the dielectric, and each period of the NP layer is controlled by the internal electric field generated by the corresponding layer of the FW. As a result, the dielectric constant ε_p changes with the internal electric field E for each NP layer in a structure with a large number of periods. This becomes quite complicated as the 1D NPPCs structure has multiple periods. The proposed scheme in this paper is based on the modulation of material refractive index under high incident intensity. The signal wave can be incident at an angle, as shown in Figure 1. In this article, the optical intensity of the FW is around 100–1000 W cm^{-2}, while the optical intensity of the CW is above 100 GW cm^{-2}. Due to the much higher amplitude of the CW compared to that of the signal wave, the influence of any nonlinear effects and internal electric field variations caused by the signal wave can be ignored. In summary, in the proposed 1D NPPCs model, the refractive index is related to the external controlling wave excitation, and the refractive index distribution of the entire NP structure has the following form:[43]

$$n_p^{(s)} = n_p^{(f)} + \Delta n_1 I \tag{7}$$

Equation (7) shows that the intensity of the cross-CW is represented by I. The schematic diagram of the structure is shown in Figure 1. Under the excitation of the CW, the refractive index of the P layer can be calculated by utilizing the optical Kerr effect, taking into account the condition of nonexistence or existence of high-intensity CW. Johnson et al.[44] and Hu et al.[45] have demonstrated the convergence and correctness of this approximation method. Kumar et al.[43] have pointed out that this method can yield correct results as long as the Kerr effect holds.

At present, the first step in generating SHW radiation can be initiated, which involves the propagation of the FW amplitude. First, the strong light interacts with the nonlinear medium, and

the relationship between P and E is nonlinear and can be expressed as follows:

$$P = \varepsilon_0 \chi^{(1)} \cdot E + \varepsilon_0 \chi^{(2)} \cdot E^2 + \varepsilon_0 \chi^{(n)} \cdot E^n + \cdots \tag{8}$$

The $\chi^{(n)}$ is the nth order electric polarizability ($n = 1, 2, 3...$). The expression can be simplified as follows:

$$P = \varepsilon_0 \chi^{(1)} \cdot E + P_{NL} \tag{9}$$

where $\boldsymbol{P}$ represents the polarization intensity, $\boldsymbol{E}$ represents the electric field intensity, P_{NL} represents the nonlinear component, and ϵ_n is the vacuum permittivity. Substituting Equation (9) into the Maxwell equations and the material equation yields the Maxwell equations for anisotropic, nonlinear, non-magnetic media:

$$\nabla \times E = -\mu_0 \frac{\partial H}{\partial t} \tag{10a}$$

$$\nabla \times H = \frac{\partial D}{\partial t} + \sigma E \tag{10b}$$

$$D = \varepsilon \cdot E + P_{NL} \tag{10c}$$

In Equation (10) μ_n represents the vacuum permeability, and σ represents the electrical conductivity, $\varepsilon = \epsilon_0[1 + \chi^{(1)}]$. The propagation equation of FW and SHW in the nonlinear medium can be expressed as follows:

$$\nabla \times \nabla \times E + \mu_0 \sigma \frac{\partial E}{\partial t} + \mu_0 \frac{\partial^2 \varepsilon \cdot E}{\partial t^2} = -\mu_0 \frac{\partial^2 P_{NL}}{\partial t^2} \tag{11}$$

Equation (11) has an additional term on the right-hand side compared to the linear equation, which corresponds to the existence of an SHW source. Assuming the medium is lossless, the equation can be simplified by setting to zero, resulting in:

$$\nabla \times \nabla \times E(r, t) + \frac{1}{\epsilon_0 c^2} \frac{\partial^2}{\partial t^2} \varepsilon \cdot E(r, t) = -\mu_0 \frac{\partial^2}{\partial t^2} P_{NL}(r, t) \tag{12}$$

where c represents the speed of light in a vacuum. Assuming a non-absorbing, homogeneous, and isotropic nonlinear medium, the vector constancy equation can be used:

$$\nabla \times \nabla \times E = -\nabla^2 E + \nabla(\nabla \cdot E) = -\nabla^2 E \tag{13}$$

Using $n = \sqrt{\varepsilon/\epsilon_0}$, the nonlinear wave equation in Equation (12) can be simplified as:

$$\nabla^2 E(r, t) - \frac{n^2}{c^2} \frac{\partial^2}{\partial t^2} E(r, t) = \mu_0 \frac{\partial^2}{\partial t^2} P_{NL}(r, t) \tag{14}$$

Henceforth, the nonlinear fluctuation equations can be derived in the form of the FW and SHW, which may be articulated as follows:

$$\nabla^2(E_f) - \frac{\varepsilon_f}{\epsilon_0 c^2} E_f = \mu_0 \frac{\partial^2}{\partial t^2} P_{NL}^f \tag{15a}$$

$$\nabla^2(E_s) - \frac{\varepsilon_s}{\epsilon_0 c^2} E_s = \mu_0 \frac{\partial^2}{\partial t^2} P_{NL}^s \tag{15b}$$

In Equation (15), ε_f, ε_s, P_{NL}^f, P_{NL}^s represent the dielectric constants and nonlinear polarizabilities at the FW and SHW frequencies. Since the nonlinear process is weak, it has little effect on the intensity of the FW. Consequently, under the assumption that the pump wave remains insignificantly affected by nonlinear processes, the fundamental electric field across all three media can be delineated as:

$$E_m^{(f)} = E_m^{f+} e^{i\left[k_r^{(f)}\left(Z - Z_{m-1}\right) - \omega t\right]} + E_m^{f-} e^{-i\left[k_r^{(f)}\left(Z - Z_{m-1}\right) - \omega t\right]} \tag{16}$$

Equation (16) employs the variable f to represent the fundamental wave (FW), with m denoting the corresponding layer number. Here, $z_m = z_{m+1} - d_m$ and $z_0 = 0$, where d_m represents the thickness of the mth layer, $k_r^{(f)} = n_r^{(f)} k_0^{(f)}$, $k_0^{(f)} = \omega/c$, ($r = a, b, c...$). $\boldsymbol{k}_r^{(f)}$ is the wave vector of the FW field in the rth layer, and $\boldsymbol{c}$ represents the speed of light in vacuum. While $E_m^{(f)+}$ and $E_m^{(f)-}$ respectively denote the complex electric field amplitudes of the forward and backward propagating waves. The application of continuity conditions for electric and magnetic fields at the layer boundaries yields the relationship between electric field amplitudes at odd and even domain interfaces in layers A and B:

$$\begin{pmatrix} E_1^+ \\ E_1^- \end{pmatrix} = \frac{1}{2n_a^{(f)}} \begin{pmatrix} n_a^{(f)} + n_b^{(f)} & n_a^{(f)} - n_b^{(f)} \\ n_a^{(f)} - n_b^{(f)} & n_a^{(f)} + n_b^{(f)} \end{pmatrix} \begin{pmatrix} E_2^+ \\ E_2^- \end{pmatrix} = T_{AB} \begin{pmatrix} E_2^+ \\ E_2^- \end{pmatrix} \tag{17}$$

Define:

$$D_A = \begin{pmatrix} 1 & 1 \\ n_a^{(f)} & -n_a^{(f)} \end{pmatrix} \tag{18a}$$

$$D_B = \begin{pmatrix} 1 & 1 \\ n_b^{(f)} & -n_b^{(f)} \end{pmatrix} \tag{18b}$$

Substitution of Equation (18) into Equation (17) followed by simplification yields:

$$T_{AB} = D_A^{(-1)} D_B \tag{19}$$

Thus, the relationship between the interfaces of the first FCs layer (A) and those of the second FCs (B) can be obtained as:

$$T_{BA} = D_B^{(-1)} D_A \tag{20}$$

The phase and amplitude variations of the pump wave at the fundamental frequency as it propagates from the left to the right of a uniform layer can be described as follows:

$$N_m = \begin{pmatrix} \exp(ik_r^{(f)} d_r) & 0 \\ 0 & \exp(-ik_r^{(f)} d_r) \end{pmatrix} \tag{21}$$

Herein, the variables $r = a$, b, and p are employed to denote the layers A, B, and P, respectively. The propagation process of the fundamental wave from the FCs (B) layer to the NP (P) layer is similar to the above process, and can be described as:

$$D_P = \begin{pmatrix} 1 & 1 \\ n_p^{(f)} & -n_p^{(f)} \end{pmatrix} \tag{22}$$

ADVANCED
SCIENCE NEWS

www.advancedsciencenews.com

annalen
der physik

www.ann-phys.org

Combining Equations (18)–(22), the overall transmission matrix of the entire nonlinear multilayer structure can be obtained by cascading the single transmission matrices of the three-layer structure within one period.

$$T = D_0^{-1} \left(D_P N_P D_P^{-1} D_B N_B D_B^{-1} D_A N_A D_A^{-1} \right)^N D_0 \tag{23}$$

Here:

$$D_0 = \begin{pmatrix} 1 & 1 \\ n_0 & -n_0 \end{pmatrix} \tag{24}$$

n_0 is the refractive index of air, thus we obtain the variation of the FW field from the left to the right of the 1D NPPCs structure, which is determined by the following matrix:

$$\begin{pmatrix} E_T^{f\,+} \\ E_T^{f\,-} \end{pmatrix} = T \begin{pmatrix} E_0^{f\,+} \\ E_0^{f\,-} \end{pmatrix} \tag{25}$$

Given the matrix T, reflection and transmission coefficients can be determined by solving for them. Therefore, the relative amplitudes of each layer in the 1D NPPCs structure can be obtained using Equation (25) under given conditions of the incident wave coefficients.

$$\begin{pmatrix} E_{3j-2}^+ \\ E_{3j-2}^- \end{pmatrix} = D_A^{(-1)} (D_P N_P D_P^{(-1)} D_B N_B D_B^{(-1)} D_A N_A D_A^{(-1)})^{j-1} D_0 \begin{pmatrix} E_0^+ \\ E_0^- \end{pmatrix} \tag{26a}$$

$$\begin{pmatrix} E_{3j-1}^+ \\ E_{3j-1}^- \end{pmatrix} = D_B^{(-1)} D_A N_A D_A^{(-1)} (D_P N_P D_P^{(-1)} D_B N_B D_B^{(-1)}$$
$$D_A N_A D_A^{(-1)})^{j-1} D_0 \begin{pmatrix} E_0^+ \\ E_0^- \end{pmatrix} \tag{26b}$$

$$\begin{pmatrix} E_{3j}^+ \\ E_{3j}^- \end{pmatrix} = D_P^{(-1)} D_B N_B D_B^{(-1)} D_A N_A D_A^{(-1)} (D_P N_P D_P^{(-1)} D_B N_B D_B^{(-1)}$$
$$D_A N_A D_A^{(-1)})^{j-1} D_0 \begin{pmatrix} E_0^+ \\ E_0^- \end{pmatrix} \tag{26c}$$

Equations (26a–c) represent the relative amplitudes in layers A, B, and P, respectively, in a 1D NPPCs structure. Here, $j = (1,2,3...N)$. It is evident that when $j = 1$, the equations above represent the relative amplitudes of the FW in each layer from the first to the third layer. The initial stage of SHG has concluded, during which the distribution of the FW amplitude within each layer of the 1D NPPCs was acquired. The next important task in the second stage is to solve the SHG. Equation (15b) describes

the nonlinear wave equation under the SHW form, solving Equation(15b) gives the SHW electric field as follows:

$$E_m^{(s)}(z) = E_m^{(s)+} \exp\left[ik_r^{(s)}(z - z_{m-1})\right] + E_m^{(s)-} \exp\left[-ik_r^{(s)}(z - z_{m-1})\right]$$
$$+ A_i \left(E_m^{(f)+}\right)^2 \exp\left[ik_r^{(f)}(z - z_{m-1})\right]$$
$$+ A_i \left(E_m^{(f)-}\right)^2 \exp\left[-ik_r^{(f)}(z - z_{m-1})\right]$$
$$+ 2C_i E_m^{(f)+} E_m^{(f)-} \tag{27}$$

where $k_r^{(s)}$ is the wave vector of the SHW field in the rth layer, $k_r^{(s)} = n_r^{(s)} k_0^{(s)}$ and $k_0^{(s)} = 2\omega/c$. $E_m^{(s)+}$ and $E_m^{(s)-}$ represent the forward and backward amplitudes of the SHW, respectively, and:

$$A_r = \frac{-4\mu\varepsilon_0 \chi_r^{(s)} \omega^2}{k_r^{(s)2} - 4k_r^{(f)2}} \quad C_r = \frac{-4\mu\varepsilon_0 \chi_r^{(s)} \omega^2}{k_r^{(s)2}} \tag{28}$$

By virtue of Maxwell's equations, the magnetic field H within each layer of the nonlinear structure can be expressed by the following equation:

$$H_m^{(s)}(z) = \frac{1}{ik_0^{(s)}} \left[\nabla \times E_m^2(z)\right] = n_r^{(s)} \left\{ E_m^{(s)+} \exp\left[ik_r^{(s)}(z - z_{m-1})\right]\right.$$
$$\left. - E_m^{(s)-} \exp\left[-ik_r^{(s)}(z - z_{m-1})\right] \right\}$$
$$+ \frac{2k_0^{(f)} n_r^{(f)}}{k_0^{(s)}} A_i \left\{ \left(E_m^{(f)+}\right)^2 \exp\left[i2k_r^{(f)}(z - z_{m-1})\right]\right.$$
$$\left. - \left(E_m^{(f)-}\right)^2 \exp\left[-i2k_r^{(f)}(z - z_{m-1})\right] \right\} \tag{29}$$

Building upon the obtained electrical and magnetic equations for SHW (Equations (27) and (29)), the propagation of SHW within the structure will now be investigated, which constitutes the third phase. The following definition applies:

$$E_m^{(s)+}(z) = E_m^{(s)+} \exp\left[ik_m^{(2)}(z - z_{m-1})\right] \tag{30a}$$

$$E_m^{(s)-}(z) = E_m^{(s)-} \exp\left[-ik_m^{(s)}(z - z_{m-1})\right] \tag{30b}$$

$$(E_m^{(f)+})^2(z) = E_m^{(f)+} \exp\left[i2k_m^{(f)}(z - z_{m-1})\right] \tag{30c}$$

$$(E_m^{(f)-})^2(z) = E_m^{(f)-} \exp\left[-i2k_m^{(f)}(z - z_{m-1})\right] \tag{30d}$$

Hence, Equations (27)–(29) can be reformulated in the following form:

$$\begin{pmatrix} E_m^{(s)}(z) \\ H_m^{(s)}(z) \end{pmatrix} = \begin{pmatrix} 1 & 1 \\ n_r^{(s)} & -n_r^{(s)} \end{pmatrix} \begin{pmatrix} E_m^{(s)+}(z) \\ E_m^{(s)-}(z) \end{pmatrix}$$
$$+ \begin{pmatrix} 1 & 1 \\ \frac{2n_r^{(f)} k_0^{(f)}}{k_0^{(s)}} & -\frac{2n_r^{(f)} k_0^{(f)}}{k_0^{(s)}} \end{pmatrix} \begin{pmatrix} A_i (E_m^{(f)+})^2(z) \\ A_i (E_m^{(f)-})^2(z) \end{pmatrix}$$
$$+ \begin{pmatrix} 1 \\ 0 \end{pmatrix} C_r E_m^{(f)+} E_m^{(f)-} \tag{31}$$

The first term on the right-hand side of Equation (31) is affected by the SHW and is expressed as a free waveguide mode, while the second term is influenced by the FW and represents the bound wave amplitude. It should be noted that it includes the forward and backward FW fields in the layer structure. The third term is influenced by the FW and represents the interference of the FW on the SH. We define several matrices as follows:

$$G_0 = \begin{pmatrix} 1 & 1 \\ n_0 & -n_0 \end{pmatrix} G_a = \begin{pmatrix} 1 & 1 \\ n_a^{(s)} & -n_a^{(s)} \end{pmatrix} \tag{32}$$

$$G_b = \begin{pmatrix} 1 & 1 \\ n_b^{(s)} & -n_b^{(s)} \end{pmatrix} G_p = \begin{pmatrix} 1 & 1 \\ n_p^{(s)} & -n_p^{(s)} \end{pmatrix} \tag{33}$$

$$B_1 = \begin{pmatrix} 1 & 1 \\ \frac{2n_a^{(f)} k_0^{(f)}}{k_0^{(s)}} & -\frac{2n_a^{(f)} k_0^{(f)}}{k_0^{(s)}} \end{pmatrix} B_2 = \begin{pmatrix} 1 & 1 \\ \frac{2n_b^{(f)} k_0^{(f)}}{k_0^{(s)}} & -\frac{2n_b^{(f)} k_0^{(f)}}{k_0^{(s)}} \end{pmatrix} \tag{34}$$

$$B_3 = \begin{pmatrix} 1 & 1 \\ \frac{2n_p^{(f)} k_0^{(f)}}{k_0^{(s)}} & -\frac{2n_p^{(f)} k_0^{(f)}}{k_0^{(s)}} \end{pmatrix} \tag{35}$$

In accordance with the boundary conditions, the SHW field on both sides of the nonlinear structure layer is matched, and the plane wave coefficients of the SHW in the air film are extracted. First, the phase and amplitude variations of the FW and SHW fields from the left to the right of the structure can be described as:

$$Q_r = \begin{pmatrix} \exp(ik_r^{(s)} d_r) & 0 \\ 0 & \exp(-ik_r^{(s)} d_r) \end{pmatrix} \tag{36a}$$

$$F_r = \begin{pmatrix} \exp(2ik_r^{(f)} d_r) & 0 \\ 0 & \exp(-2ik_r^{(f)} d_r) \end{pmatrix} \tag{36b}$$

In this equation, $r = (a, b, p)$. The relationship between the left side of the SHW field strength in the structure and the SHW and FW amplitudes can be expressed as:

$$G_r \begin{pmatrix} E_{m-1}^{(s)+}(z) \\ E_{m-1}^{(s)-}(z) \end{pmatrix} = G_r \begin{pmatrix} E_m^{(s)+} \\ E_m^{(s)-} \end{pmatrix} + B_i \begin{pmatrix} A_i (E_m^{(f)+})^2 \\ A_i (E_m^{(f)-})^2 \end{pmatrix} + \begin{pmatrix} C_r \\ 0 \end{pmatrix} E_m^{(f)+} E_m^{(f)-} \tag{37}$$

For the right side of this layer in the structure, the relationship between the strength of the SHW field and the SHW and FW amplitudes is:

$$G_0 \begin{pmatrix} E_{m-1}^{(s)+}(z) \\ E_{m-1}^{(s)-}(z) \end{pmatrix} = G_r Q_r \begin{pmatrix} E_m^{(s)+} \\ E_m^{(s)-} \end{pmatrix} + B_i F_r \begin{pmatrix} A_r (E_m^{(f)+})^2 \\ A_r (E_m^{(f)-})^2 \end{pmatrix} + \begin{pmatrix} C_r \\ 0 \end{pmatrix} E_m^{(f)+} E_m^{(f)-} \tag{38}$$

The interrelation between the SHW at the two interfaces of the nonlinear medium layer can be obtained by utilizing Equations (37), (38).

$$\begin{pmatrix} E_{m-1}^{(s)+}(z) \\ E_{m-1}^{(s)-}(z) \end{pmatrix} = G_0^{(-1)} N_r G_0 \begin{pmatrix} E_m^{(s)+} \\ E_m^{(s)-} \end{pmatrix}$$

$$+ G_0^{(-1)} (B_r F_r - N_r B_r) \begin{pmatrix} A_r (E_m^{(f)+})^2 \\ A_r (E_m^{(f)-})^2 \end{pmatrix} \tag{39}$$

$$+ G_0^{(-1)} (1 - N_r) \begin{pmatrix} C_r \\ 0 \end{pmatrix} E_m^{(f)+} E_m^{(f)-}$$

Equation (39) is the SHG relationship equation for the single layer structure. Considering that the overall structure is periodic, the aforementioned equation may be employed as a recursive equation to obtain the global matrix for SHG in the 1D NPPCs structure over the first period.

$$\begin{pmatrix} E_3^{(s)+}(z) \\ E_3^{(s)-}(z) \end{pmatrix} = G_0^{(-1)} S G_0 \begin{pmatrix} E_0^{(s)+} \\ E_0^{(s)-} \end{pmatrix}$$

$$+ G_0^{(-1)} (N_1 B_1 F_1 - S B_1) \begin{pmatrix} A_a (E_{3s-2}^{(f)+})^2 \\ A_a (E_{3s-2}^{(f)-})^2 \end{pmatrix} + G_0^{(-1)} (N_1 - S) \begin{pmatrix} C_a \\ 0 \end{pmatrix} E_{3s-2}^{(f)+} E_{3s-2}^{(f)-}$$

$$+ G_0^{(-1)} (N_2 B_2 F_2 - N_1 B_1) \begin{pmatrix} A_b (E_{3s-1}^{(f)+})^2 \\ A_b (E_{3s-1}^{(f)-})^2 \end{pmatrix} + G_0^{(-1)} (N_2 - N_1) \begin{pmatrix} C_b \\ 0 \end{pmatrix} E_{3s-1}^{(f)+} E_{3s-1}^{(f)-}$$

$$+ G_0^{(-1)} (B_2 F_2 - N_2 B_1) \begin{pmatrix} A_p (E_{3s}^{(f)+})^2 \\ A_p (E_{3s}^{(f)-})^2 \end{pmatrix} + G_0^{(-1)} (1 - N_2) \begin{pmatrix} C_p \\ 0 \end{pmatrix} E_{3s}^{(f)+} E_{3s}^{(f)-} \tag{40}$$

**ADVANCED
SCIENCE NEWS**

www.advancedsciencenews.com

annalen
der **physik**

www.ann-phys.org

Here:

$$S = G_p Q_p G_p^{(-1)} G_b Q_b G_b^{(-1)} G_a Q_a G_a^{(-1)} N_1 = G_p Q_p G_p^{(-1)} G_b Q_b G_b^{(-1)} N_2$$

$$= G_p Q_p G_p^{(-1)} \tag{41}$$

The employment of Equation (40) enables the acquisition of the SHW transfer matrix of the entire 1D NPPCs structure comprising N periodic units. The following equation can be used to obtain the SHW field that passes through the right-hand side and reflects from the left-hand side:

$$\begin{pmatrix} E_T^{(s)+} \\ 0 \end{pmatrix} = G_0^{(-1)} S^N G_0 \begin{pmatrix} 0 \\ E_0^{(s)-} \end{pmatrix}$$

$$+ \sum_{s=0}^{N} G_0^{(-1)} S^{N-s} \left[(N_1 B_1 F_1 - S B_1) \begin{pmatrix} A_a (E_{3s-2}^{(f)+})^2 \\ A_a (E_{3s-2}^{(f)-})^2 \end{pmatrix} + (N_1 - S) \begin{pmatrix} C_a \\ 0 \end{pmatrix} E_{3s-2}^{(f)+} E_{3s-2}^{(f)-} \right.$$

$$+ (N_2 B_2 F_2 - N_1 B_1) \begin{pmatrix} A_b (E_{3s-1}^{(f)+})^2 \\ A_b (E_{3s-1}^{(f)-})^2 \end{pmatrix} + (N_2 - N_1) \begin{pmatrix} C_b \\ 0 \end{pmatrix} E_{3s-1}^{(f)+} E_{3s-1}^{(f)-}$$

$$\left. + (B_2 F_2 - N_2 B_1) \begin{pmatrix} A_p (E_{3s}^{(f)+})^2 \\ A_p (E_{3s}^{(f)-})^2 \end{pmatrix} + (1 - N_2) \begin{pmatrix} C_p \\ 0 \end{pmatrix} E_{3s}^{(f)+} E_{3s}^{(f)-} \right] \tag{42}$$

The generation of SHW radiation can be attributed to the mutual interaction between the FW and the nonlinear medium in each layer, as inferred from Equation (42). The excitation of the SHG is governed by the intensity of the FW within each layer, as well as the second-order nonlinear coefficient, which is a crucial factor in the process. Consequently, the pursuit of materials with elevated nonlinear coefficients represents a critical avenue for enhancing the SHW total conversion efficiency (T-con).

The methods for computing the forward and backward SHW amplitudes in the 1D NPPCs structure have been established. However, measuring the SHW amplitudes directly in experiments is often challenging. Therefore, it is proposed to utilize the calculation of SHG intensity as a substitute. The forward transmission T-con and backward reflection T-con are defined based on the wave intensity, which takes the following form:

$$\eta_t = \frac{I_t^{(s)+}}{I_0^{(f)}} \tag{43}$$

$$\eta_r = \frac{I_r^{(s)-}}{I_0^{(f)}} \tag{44}$$

The T-con of the SHW in the 1D NPPCs structure can be obtained through Equations (43), (44):

$$\eta = \eta_t + \eta_r \tag{45}$$

3. Investigation and Discussion

As is well known, in nonlinear structures, the size of the T-con of SHW depends on the value of the second-order nonlinear coefficient and the pump light intensity. In contrast, this article has opted for SBN crystals with relatively high nonlinear coefficients. In this case, achieving higher conversion efficiency depends on adjusting the phase difference between FW and SHW. By adjusting the phase difference between the FW and the SHW, it is possible to optimize the coherent superposition effect and phase matching, thereby achieving higher SHW T-con.[46,47] Since it is impossible to achieve perfect phase matching in the 1D NPPCs structure, QPM is undoubtedly the optimal solution for obtaining higher SHW output intensity.

In this study, numerical simulations are performed to establish the QPM conditions in a 1D NPPC structure by adjusting the thickness d_b of the B layer, the FW frequency f_{FW}, and the phase-matching angle θ. To further analyze the frequency doubling effect of the structure, the initial parameters are set as follows: $d_a = 336.3$ mm, $d_p = 84.8$ mm, $n_a^{(f)} = 1.617$, $n_b^{(f)} = 2.955$, $n_a^{(s)} = 1.68$, $n_b^{(s)} = 3.245$, $n_p^{(f)} = 1.5$, $\Delta n_1 = 1.6 \times 10^{-13} cm^2$ W^{-1}, $I = 3.12501 \times 10^3$ GW cm^{-2}. The generation of the optimal structure is linked to the maximum value of the T-con of the frequency doubling wave. In **Figure 2**, when the thickness of the B-layer d_b is adjusted to 206.5 mm, the maximum value of the T-con of SHW is $\eta = 20.62\%$. At this point, the frequency of the FW is $f_{FW} = 22.84$ GHz, and the phase difference between FW and SHW is minimized. By utilizing this structured design, different light beams can propagate along different paths in the photonic crystal, generating SHW at the position of phase matching. Finally, through the definition of the optimal structure, the structure consists of 40 stacked layers, and the SHG conversion intensity exceeds 20%. This result is significant without considering the pump light intensity and the external CW of the NP layer structure.

To investigate the magnitudes of forward transmitted and backward reflected waves during the SHG process, the calculated efficiency results around $d_b = 206.5$ mm are shown in **Figures 3**a and 3b, respectively. The nonlinear structural parameters are the same as in Figure 2. Figures 3a and 3b show the output efficiency
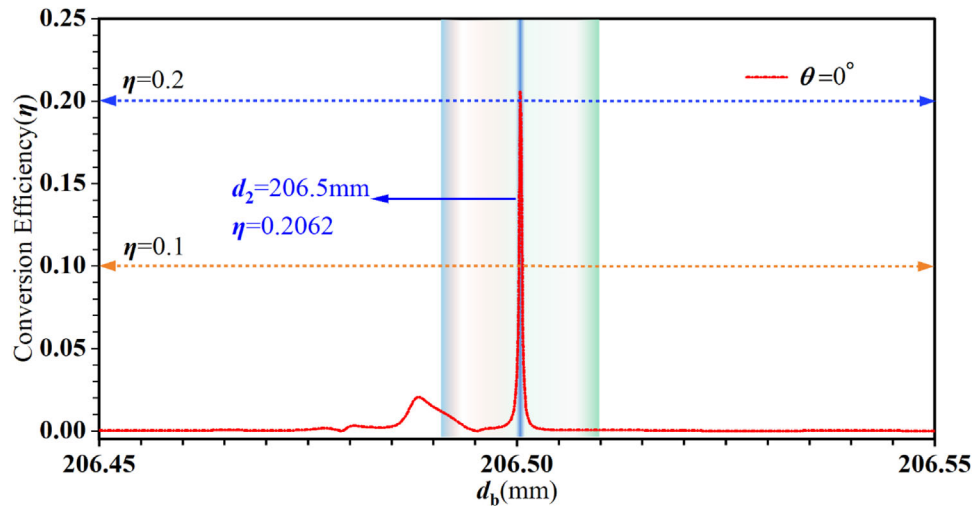
**ADVANCED
SCIENCE NEWS**

www.advancedsciencenews.com

annalen
der **physik**

www.ann-phys.org

Figure 2. The relationship between the T-con (η) and the thickness d_b of the SBN crystal layer B. The $\theta = 0°$ and the frequency of the FW is 22.84 GHz.
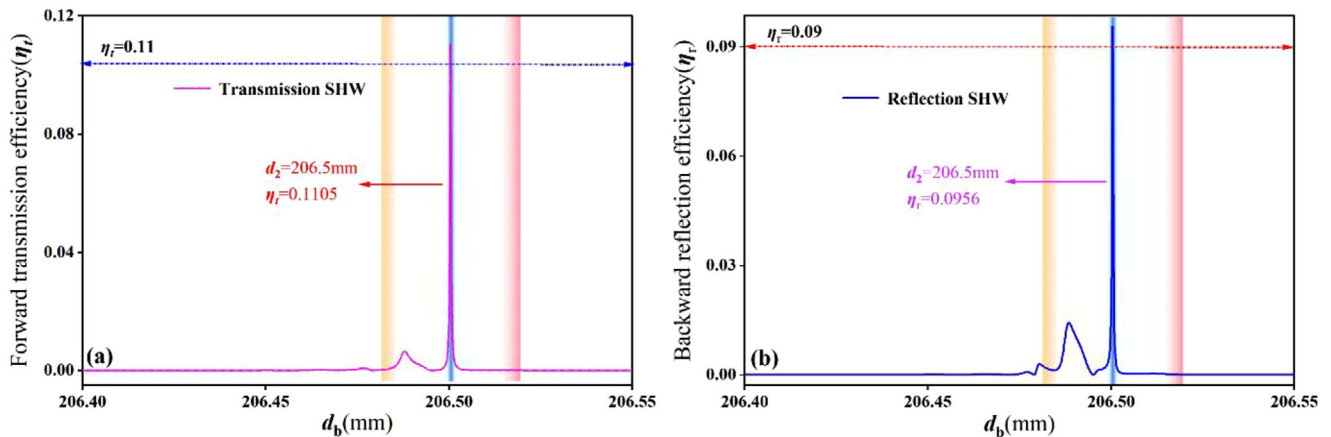

Figure 3. The forward transmission efficiency of a) the SHW and b) the backward reflection efficiency of the SHW are shown.

of the forward transmitted wave and the backward reflected wave during the SHG process, respectively, with the forward output intensity $\eta_t = 11.05\%$ and the backward output intensity $\eta_r = 9.56\%$. The results indicate that the 1D NPPCs structure has significant radiation in both forward and backward directions during the propagation of SHW, and the intensities of the transmitted and reflected waves are approximately equal. This is due to the multiple reflection effect caused by the large refractive index discontinuity, which enhances the backward signal and further increases the T-con value. It should be noted that the SHG in the structure will only be continuously enhanced when there is complete phase matching.

The transmission spectra for the case where $\theta = 0°$ and the thickness of layer B is 206.5 mm are shown in **Figure 4**. Figure 4a shows the transmission spectrum of the FW, while Figure 4b shows that of the SHW. By observation, it can be seen that the FW frequency f_{FW} is tuned to the edge of the PBG in Figure 4a, while the SHW frequency is relatively close to the band edge in Figure 4b. The structural parameters are the same as those in Figure 2. The results indicate that selecting the pump wave fre-

quency of 22.84 GHz is an important condition for obtaining optimal structure. This selection results in the strong reflection and scattering of the FW within the structure, prolonging its interaction time with the nonlinear medium. As a consequence, it leads to a higher density of electromagnetic field modes and a smaller group velocity.[42,48] Under these conditions, the field amplitude is enhanced by at least one order of magnitude, and the nonlinear interaction time in the structure becomes longer. These factors are the key to significantly improving the T-con.

To verify the significance of parameter tuning at the PBG edge, we have plotted the transmission spectra of FW (fundamental wave) and SHW (second harmonic wave) under different θ values, considering TM polarization conditions. As shown in **Figure 5**, for $\theta = 15°$, $\theta = 45°$, and $\theta = 60°$. The refractive index and thickness parameters of the structure were chosen to be the same as those in Figure 2. In Figures 5a, 5c, and 5e, it can be observed that the frequency of FW is closer to the PBG edge for $\theta = 45°$ than for $\theta = 15°$, and when the θ is changed to 60°, the FW frequency is tuned to a frequency far from the PBG. In Figures 5b, 5d, and 5f, the frequency of the SHW is almost the same distance
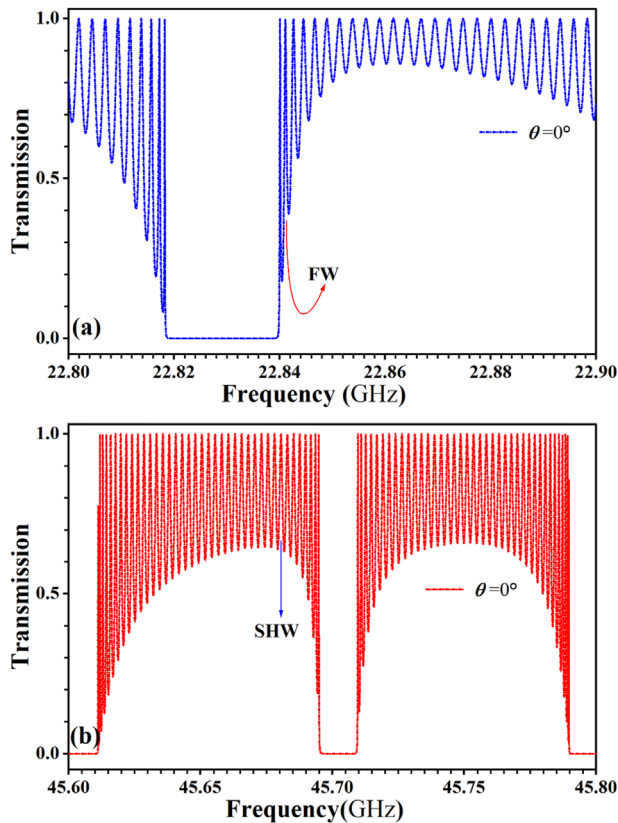
**ADVANCED
SCIENCE NEWS**

www.advancedsciencenews.com

annalen
der **physik**

www.ann-phys.org

Figure 4. The transmission spectra around the wavelengths of a) the FW and b) SHW fields when the thickness of the layer B is 206.5 mm.

from the PBG as the incident angle changes. Based on these conditions, it can be concluded that the distance between the FW frequency and the PBG edge decreases in the order of $\theta = 45°$, $\theta = 15°$, and $\theta = 60°$. The SHW frequency is less affected by the incident angle and remains close to the PBG edge.

To correspond to the transmittance spectra obtained in Figure 5, **Figure 6** plots the function graph between the SHW's T-con and thickness d_b under different θ of incident waves. Compared with Figure 3, it does not include the forward and backward conversion efficiencies, only the T-con is compared. In Figure 6a, η exceeds 20% under the condition of direct incidence, which is consistent with Figure 2. When $\theta = 15°$, the η reaches 3%, when $\theta = 45°$, the η is 6%, and when $\theta = 60°$, the η is too small, which can be observed from its image in Figure 6b, where the η is only 0.5%. It is already very small. It should be noted that when drawing the relationship between η and d_b under multiple angle changes, the maximum T-con will not occur at the fixed value of 206.5 mm. With the change of θ, the optimal parameters of the 1D NPPCs structure will be biased to some extent. At this time, the best structure should be reconstructed through numerical simulation. As shown in Figure 6, under the premise of maximizing the T-con, when θ is respectively set to 15°, 45°, and 60°, d_b becomes 206.537 mm, 206.534 mm, and 206.479 mm, respectively. If the length of the B medium is fixed at 206.5 mm, the final T-con value when the pump wave is obliquely incident will decrease.

In Figure 6, when the thickness is fixed at 206.5 mm, the values of η for different incident angles are all less than 5%, and when $\theta = 60°$, η is almost zero. By comparing the sizes of η under different θ conditions, we found that η is maximum at $\theta = 0°$, followed by $\theta = 45°$, $\theta = 15°$, and $\theta = 60°$. In addition, the transmission spectrum in Figure 5 has already revealed the distance between the FW frequency band and the PBG for different θ angles. Upon comparing the results depicted in Figures 5 and 6, it can be inferred that the SHG effect in the 1D NPPCs structure becomes more pronounced as the FW frequency approaches the edge of the PBG. This can be explained by the fact that under the influence of the PBG, the state density of the FW field is high, the group velocity is low, and the local field is enhanced. These results and analyses indicate that adjusting the FW frequency to the PBG edge is an important condition for constructing the optimal nonlinear structure, and the farther away from the PBG edge, the smaller the output peak of the SHW.

To observe the internal electric field distribution of the nonlinear structure more intuitively, the simulation results of the electric field distribution of the fundamental and second harmonic with the FW frequency of about 22.84 GHz are presented by fixing the structure parameters at the maximum SHW T-con. **Figure 7**a shows the electric field distribution of the fundamental, where the energy of the electric field is distributed in a peak shape. In contrast, as shown in Figure 7b, the energy of the electric field is distributed in the shape of two peaks in the 1D NPPCs. Since the structure satisfies the QMP condition, that is, enhancing the strength and directionality of the nonlinear effect through phase control, when the optimal structure condition is reached, the electric field energy in the structure is continuously enhanced. The results show that during the FW propagation process, the interaction between the forward electromagnetic wave and the multiple reflected electromagnetic waves causes an interference effect, resulting in the oscillation of the pump field inside the structure, thereby enhancing the electric field amplitude.

It is well known that high optical intensities are often required to generate high-frequency waves in the process of SHG under the condition of QPM. **Figure 8** shows the enhancement of the frequency doubling effect with the change of FW intensity I_{FW}, under the condition of establishing a structure that satisfies the QPM condition and achieves a larger η value. It can be seen from the Figure 8 that when the light intensity I_{FW} exceeds 6×10^2 W cm^{-2}, linear fitting is achieved. The value of η is positively correlated with the intensity of the FW, and when I_{FW} exceeds 10^3 W cm^{-2}, the value of η exceeds 40%.

In the 1D NPPCs structure, the external CW of NP exists as a modulator of the refractive index of the P layer structure. To find an appropriate CW intensity that yields a strong SHG effect, **Figure 9** depicts the relationship between the optical field intensity I of CW and η, where the basic parameters are the same as those in Figure 2. It is found from the graph that multiple peaks are formed in the range of CW intensity values from 10^2 to 10^4 GW cm^{-2}. Among them, the initial peak value exceeds 45%, and as I increases, the value of η gradually decreases, eventually falling below 5%. When I is lower than I_1, the modulation of refractive index will be minimal, and the FW and SHW refractive indices of the medium layer P will become the same. In this situation, the T-con will not increase.
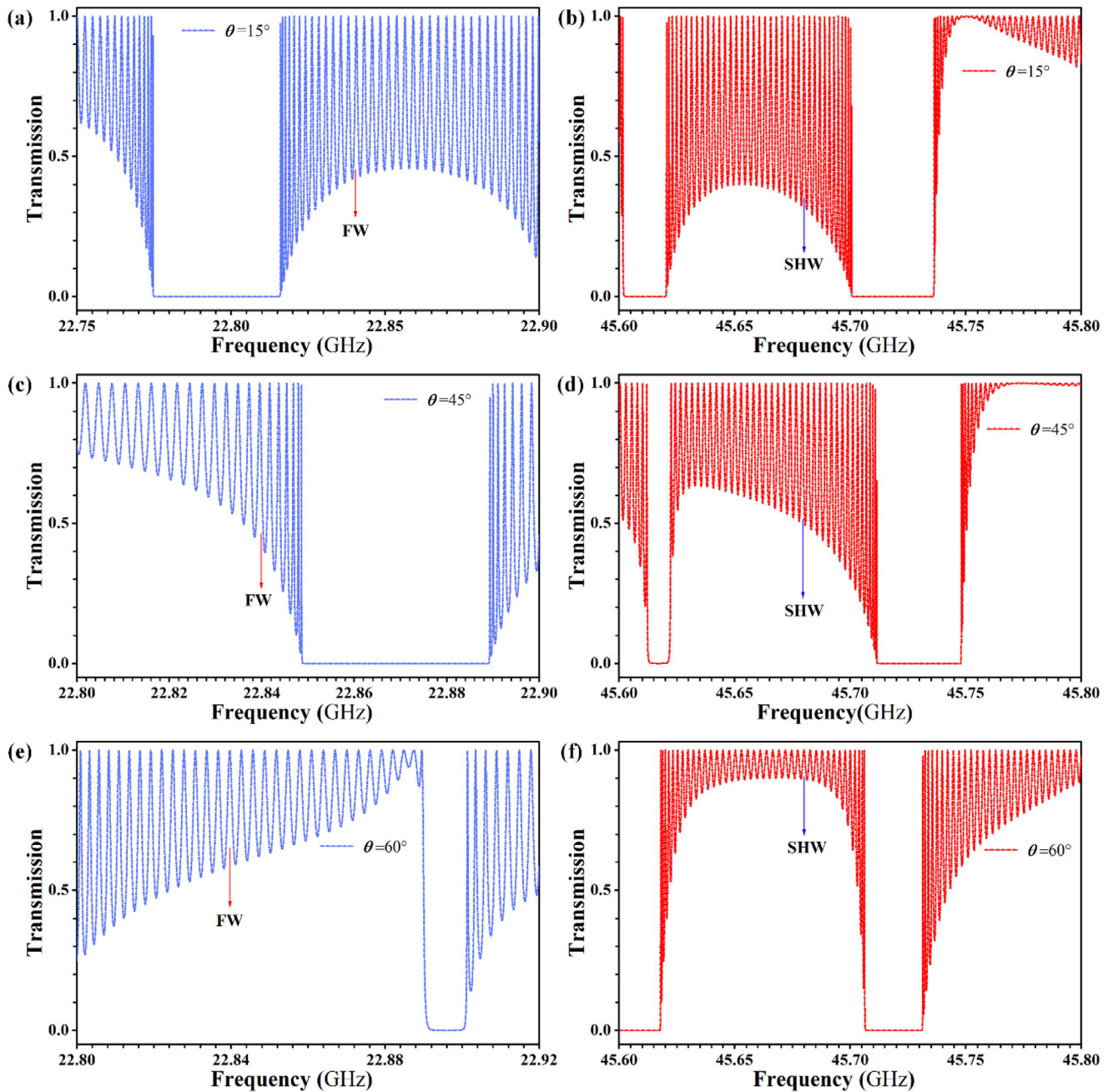
Figure 5. The transmission spectra of a) FW and b) SHW under the $\theta = 15°$, as well as the transmission spectra of c) FW and d) SHW under the $\theta = 45°$, and the transmission spectra of e) FW and f) SHW under the $\theta = 60°$under TM waves.

Table 1 records in detail the CW intensity I at representative peaks I_1 to I_{11} and their corresponding SHW η values in Figure 9. Based on Table 1, I_4 in Figure 9 represents the CW intensity of 3.12501×10^3 GW cm^{-2} selected when constructing the optimal structure in Figure 2, and η at this time is 20.62%. The changes in the optical intensity indicated by the abscissa around I_4 lead to the peak value appearing with a certain periodic distribution. Considering that each CW variation will result in a fine-tuning of the refractive index of the NP layer, which will cause the PBG to move, each high peak value represents the PBG being moved around the SHW frequency, while each low peak value represents the PBG being moved to the far-off frequency band from the SHW frequency. When the modulation of I causes the frequency of the fundamental wave to be within or far from the PBG, η is almost zero. As shown in Figure 9, if the CW intensity near the peak value is used to control the NP layer structure, it will result in the failure of phase matching, thereby greatly reducing the value of η.
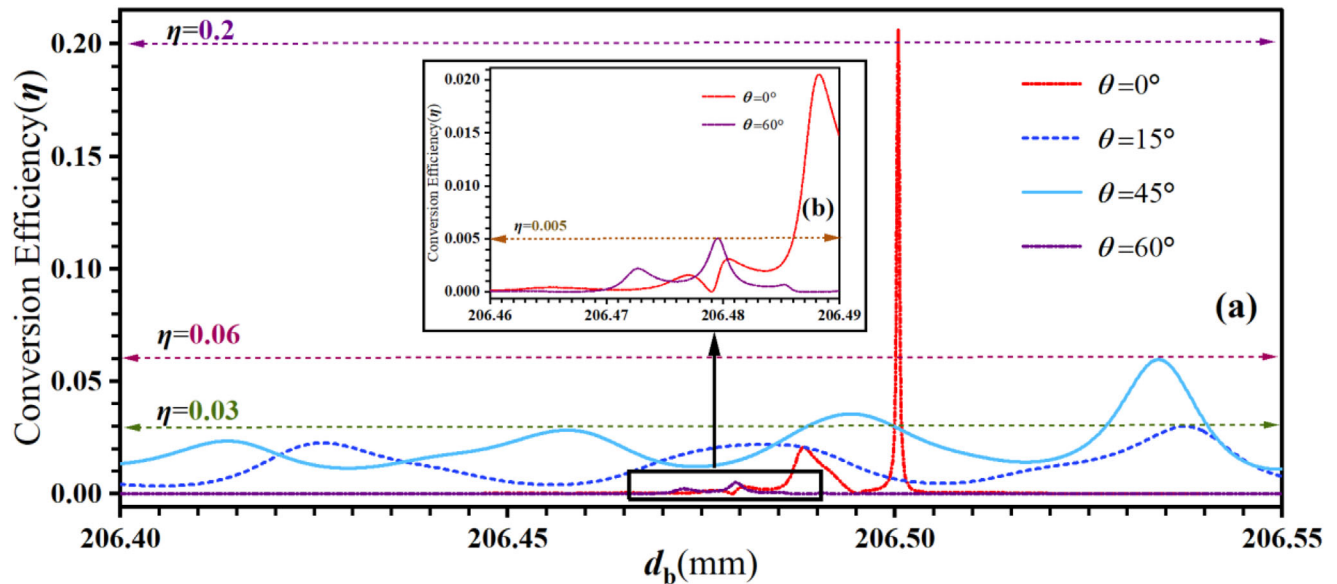
**ADVANCED
SCIENCE NEWS**

www.advancedsciencenews.com

annalen
der **physik**

www.ann-phys.org

Figure 6. The SHW's T-con graph under different incident angles, where the incident wave frequency is 22.84 GHz. When $\theta = 60°$, T-con is relatively small and can be represented using (b).
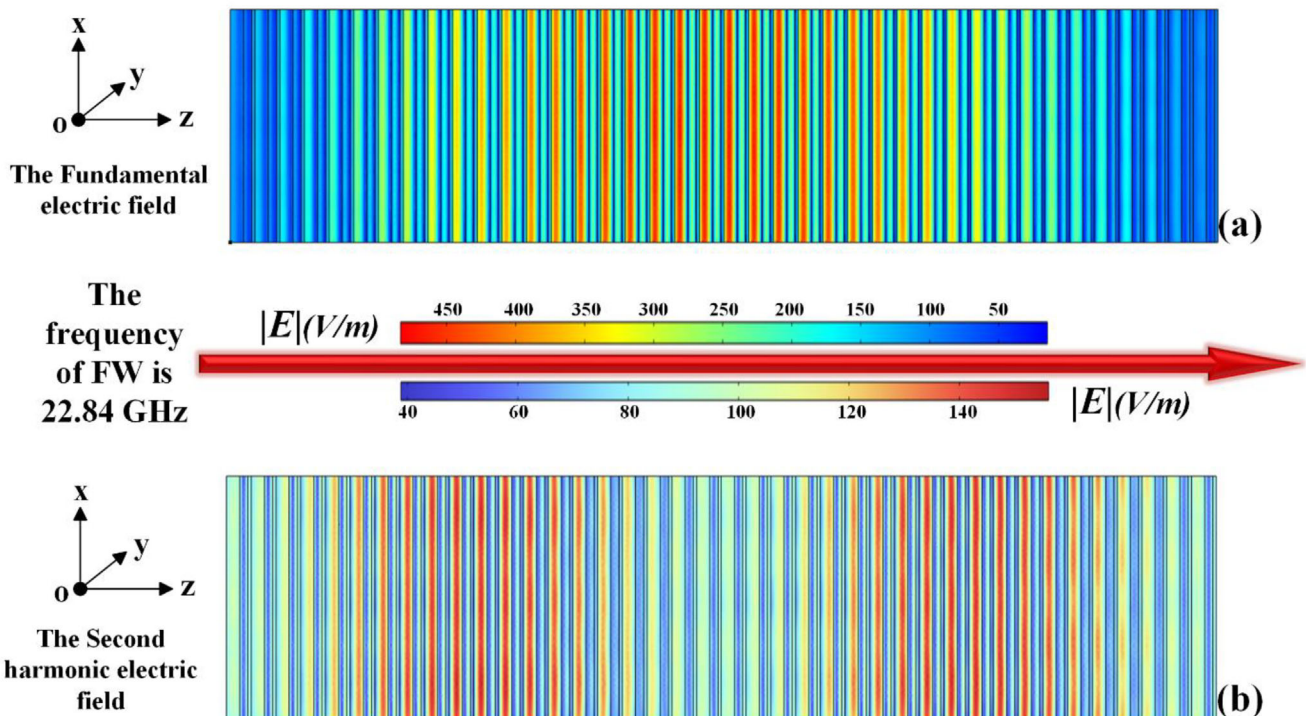

Figure 7. Schematic diagrams of the electric field distributions of a) the FW and b) SHW.

To directly observe the size of η under different CW intensities, the relationship between η and the B-layer dielectric thickness was plotted in **Figure 10**. The structural thickness d_b remained at 206.5 mm. Different SHW conversion intensities were obtained under different CW controls. Combined with the results in Table 1, it can be seen that at I_4 in the figure, where $\eta = 20.62\%$, the structural parameters of the 1D-NPPCs were the same as in

Figure 2. When the CW intensity was increased to $I_5 = 4.09781 \times 10^3$ GW cm^{-2}, $I_6 = 5.07007 \times 10^3$ GW cm^{-2}, $I_7 = 6.04187 \times 10^3$ GW cm^{-2} the value of η decreased to 16.11%, 12.3%, 9.3%. When the CW intensity was reduced to $I_3 = 2.1516 \times 10^3$ GW cm^{-2}, $I_2 = 1.17746 \times 10^3$ GW cm^{-2}, and $I_1 = 0.20249 \times 10^3$ GW cm^{-2}, the value of η successively reached 27.63%, 35.6%, and 47.17%, which was significant. The above research shows that the optimal
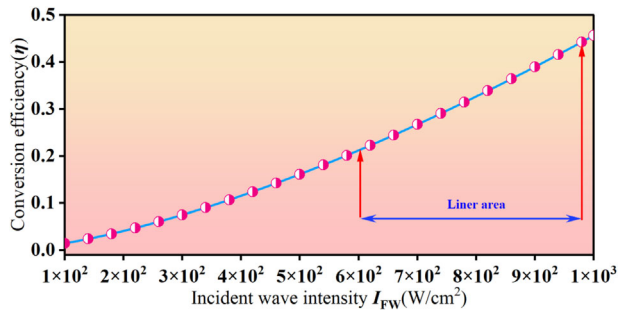
**ADVANCED
SCIENCE NEWS**

www.advancedsciencenews.com

*annalen
der* **physik**

www.ann-phys.org

Figure 8. Incident wave intensity I_{FW} versus η. The straight line in the figure is the result of a linear fit.
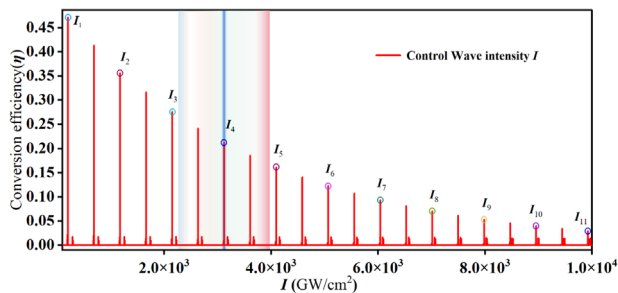

Figure 9. T-con versus CW intensity I of the NP. At this point $\theta = 0°$, the FW frequency is 22.84 GHz and the structure B thickness d_b is fixed at 206.5 mm.

structure can be achieved when the refractive index modulation of the NP layer is adjusted to the best state at $I_1 = 0.20249 \times 10^3$ GW cm^{-2}, which proves that high SHG effects can also be achieved with low refractive index modulation.

To demonstrate the significant innovation in generating SHW using 1D-NNPCs, **Table 2** presents specific parameters comparing this work with previous research results. The table includes the working frequency range, external variables, and corresponding performance parameters for different studies. On one hand, our work combines SBN crystals with NP materials and extends the generation of SHW to the GHz range, which has been rarely discussed in published articles. On the other hand, we discuss the effects of several variables, such as structural thickness, angle, and external CW, on the SHW T-con. In contrast to existing works that mainly focus on studying the impact of thickness or angle on phase matching in a monotonic manner, this work introduces discussions on the incident angle and CW variable, providing new insights into achieving higher phase matching between FW and SHW. Finally, a significant improvement in SHW T-con

Table 2. Comparison with published reports.

Refs.	Working frequency band [GHz]	External variables	Performance parameters[a]
[42]	None	Dielectric thickness	$\eta = 8\%$
[48]	None	None	$\eta = 18\%$
[49]	None	Angle	$\eta = 24\%$
[50]	None	Dielectric thickness	$\eta = 30\%$
This work	Yes	① Dielectric thickness② Angle③ CW intensity	$\eta = 47.17\%$

[a] η = SHW T-con.

has been achieved, surpassing the T-con of previous research under lower CW modulation.

4. Conclusions

In summary, this article presents the 1D NPPCs structure based on QPM. The nonlinear transfer matrix method was used to analyze the SHG problem in the nonlinear structure and to derive the transmission matrix of the periodic structure. In the nonlinear structure, the NP structure is controlled by external CW modulation, so the effect of the internal electric field can be ignored. SBN crystal with a large nonlinear coefficient was selected, which is also subject to electric field modulation. By adjusting the structural parameters, the optimal configuration with the maximum SHG efficiency has been obtained, with the FW frequency of 22.84 GHz and the T-con exceeding 20% when the CW intensity is 3.12501×10^3 GW cm^{-2}. Due to the strong scattering effect of the nonlinear PCs, the reverse SHG is enhanced, which is comparable to the forward SHG. The transmission spectra of the FW and SHW under different θ were also studied, and it was found that the T-con is smaller when the FW is farther away from the PBG edge. This is because the density of states is large near the PBG edge, and the group velocity is small, which enhances the local field. By enhancing the intensity of the incident wave, a high SHG effect can be obtained. From the perspective of QMP conditions, the electric field distribution of FW and SHW in the 1D NPPCs structure and the enhancement effect of the incident wave intensity control on SHG were studied. The interference effect of the backward reflected wave is the key to enhancing the electric field amplitude. Under the premise of obtaining the optimal structure, it was demonstrated that the PBG can also be controlled by lowering the refractive index modulation. When the CW intensity is changed to 0.20249×10^3 GW cm^{-2}, T-con exceeds 40%. This structure can be

Table 1. Corresponding values of CW intensity and η when taking the peak at I_1–I_{11} in Figure 9.

Peak	I_1	I_2	I_3	I_4	I_5	I_6
Light intensity I [$\times 10^3$ GW cm^{-2}]	0.20249	1.17746	2.1516	3.12501	4.09781	5.07007
T-con η	47.17%	35.6%	27.63%	20.62%	16.11%	12.3%
Peak	I_7	I_8	I_9	I_{10}	I_{11}	
Light intensity I [$\times 10^3$ GW cm^{-2}]	6.04187	7.01328	7.98433	8.95508	9.92555	
T-con η	9.33%	7.06%	5.31%	3.98%	2.97%	

**ADVANCED
SCIENCE NEWS**

www.advancedsciencenews.com
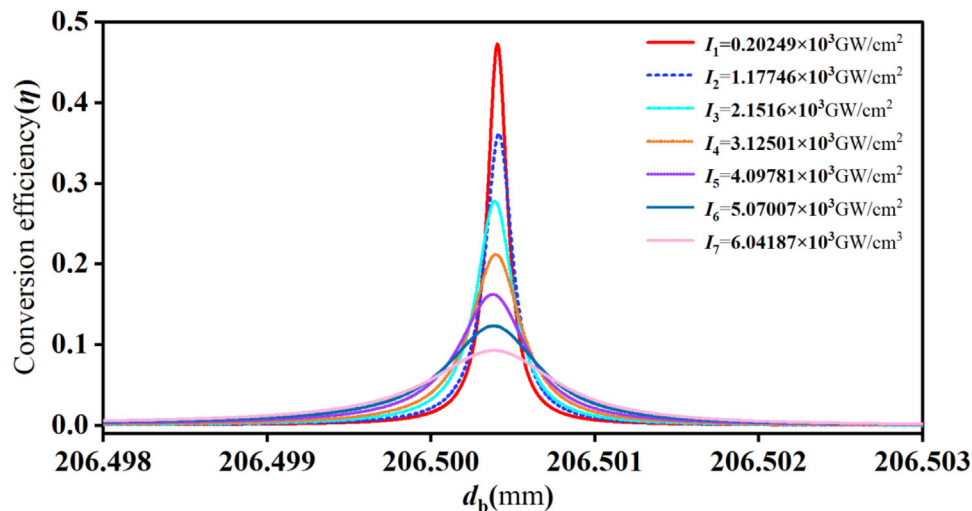
annalen
der **physik**

www.ann-phys.org

Figure 10. η versus media B thickness d_b for different CW strength conditions.

applied to areas such as communication and signal modulation. Considering that nonlinear plasma can work in the THz band under specific conditions, our nonlinear structure could verify experimentally. Of course, adjusting the operating frequency range of SBN to the GHz band poses a significant challenge, and our study provides direction for SBN future research.

Acknowledgements

Conflict of Interest

The authors declare no conflict of interest.

Data Availability Statement

The data that support the findings of this study are available on request from the corresponding author. The data are not publicly available due to privacy or ethical restrictions.

Keywords

[1] L. Kang, Y. Cui, S. Lan, S. P. Rodrigues, M. L. Brongersma, W. Cai, *Nat. Commun.* **2014**, *5*, 4680.

[2] T. Perani, D. Aurelio, M. Liscidini, *Opt. Lett.* **2019**, *44*, 5133.

[3] S. S. Rao, J. T. Zhang, H. F. Zhang, *Results Phys.* **2021**, *31*, 105058.

[4] O. Rusyakina, T. Geernaert, M. Loyez, M. Lobry, K. Chah, P. Mergo, H. Thienpont, C. Caucheteur, F. Berghmans, T. Baghdasaryan, *Sens. Actuators, B* **2023**, *382*, 133561.

[5] Y. Liang, Z. Liang, Z. Liu, P. Jun, D. Qiu, *Opt. Express* **2023**, *31*, 776.

[6] H. Mehdian, Z. Mohammadzahery, A. Hasanbeigi, *J. Phys. D: Appl. Phys.* **2015**, *48*, 305101.

[7] H. Hojo, A. Mase, *Purazuma·Kaku Yugo Gakkaishi* **2004**, *80*, 89.

[8] O. Sakai, T. Sakaguchi, K. Tachibana, *Appl. Phys. Lett.* **2005**, *87*, 241505.

[9] T. Ott, M. Bonitz, *Phys. Rev. Lett.* **2011**, *107*, 135003.

[10] S. V. Gaponenko, D. V. Novitsky, D. V. Guzatov, *Phys. Scr.* **2023**, *98*, 045614.

[11] L. Shiveshwari, P. Mahto, *Solid State Commun.* **2006**, *138*, 160.

[12] Y. Liu, W. Chen, W. Zhang, C. Q. Ma, H. X. Chen, Y. F. Xiong, R. Yuan, J. Tang, P. Chen, W. Hu, *Adv. Opt. Mater.* **2022**, *10*, 2101098.

[13] S. S. Rao, Y. Zhou, B. F. Wan, H. F. Zhang, *IEEE J. Sel. Top. Quantum Electron.* **2022**, *29*, 5100808.

[14] D. W. Wang, H. T. Zhou, M. J. Guo, J. X. Zhang, J. Evers, S. Y. Zhu, *Phys. Rev. Lett.* **2013**, *110*, 093901.

[15] S. F. Mingaleev, Y. S. Kivshar, *Phys. Rev. Lett.* **2001**, *86*, 5474.

[16] Y. Benachour, *J. Nonlinear Opt. Phys. Mater.* **2023**, *32*, 2350007.

[17] A. Arie, N. Voloch, *Laser Photonics Rev.* **2010**, *4*, 355.

[18] M. Soljacic, M. Ibanescu, C. Luo, S. G. Johnson, S. Fan, Y. Fink, J. D. Joannopoulos, *Photonic Crystal Mater. Devices* **2003**, *5000*, 200.

[19] M. Lazoul, A. Boudrioua, L. M. Simohamed, L. H. Peng, *Opt. Lett.* **2015**, *40*, 1861.

[20] J. Trull, R. Vilaseca, J. Martorell, R. Corbalan, *Opt. Lett.* **1995**, *20*, 1746.

[21] X. Luo, T. Ishihara, *Adv. Funct. Mater.* **2004**, *14*, 905.

[22] M. Arbore, O. Marco, M. Fejer, *Opt. Lett.* **1997**, *22*, 865.

[23] J. Wu, T. Kondo, R. Ito, *J. Lightwave Technol.* **1995**, *13*, 2075.

[24] R. Eckardt, J. Reintjes, *IEEE J. Quantum Electron.* **1984**, *20*, 1178.

[25] A. Chowdhury, L. McCaughan, *IEEE Photonics Technol. Lett.* **2000**, *12*, 486.

[26] P. Xu, S. Ji, S. Zhu, X. Yu, J. Sun, H. Wang, J. He, Y. Zhu, N. Ming, *Phys. Rev. Lett.* **2004**, *93*, 133904.

[27] P. Ni, B. Ma, X. Wang, B. Cheng, D. Zhang, *Appl. Phys. Lett.* **2003**, *82*, 4230.

[28] L. E. Myers, R. Eckardt, M. M. Fejer, R. L. Byer, W. R. Bosenberg, *Opt. Lett.* **1996**, *21*, 591.

[29] A. Piskarskas, V. Smilgevičius, A. Stabinis, V. Jarutis, V. Pašiškevičius, S. Wang, J. Tellefsen, F. Laurell, *Opt. Lett.* **1999**, *24*, 1053.

[30] V. N. Tsytovich, *Phys.-Usp.* **1967**, *9*, 805.

[31] O. Sakai, T. Sakaguchi, K. Tachibana, *J. Appl. Phys.* **2007**, *101*, 073304.

[32] O. Sakai, K. Tachibana, *IEEE Trans. Plasma Sci.* **2007**, *35*, 1267.

[33] O. Sakai, K. Tachibana, *Plasma Sources Sci. Technol.* **2012**, *21*, 013001.

[34] S. Y. Lin, V. Hietala, L. Wang, E. Jones, *Opt. Lett.* **1996**, *21*, 1771.

[35] F. F. Ren, R. Li, C. Cheng, H. T. Wang, J. Qiu, J. Si, K. Hirao, *Phys. Rev. B* **2004**, *70*, 245109.

[36] P. Delaye, M. Astic, R. Frey, G. Roosen, *J. Opt. Soc. Am. B* **2005**, *22*, 2494.

[37] J. Danckaert, K. Fobelets, I. Veretennicoff, G. Vitrant, R. Reinisch, *Phys. Rev. B* **1991**, *44*, 8214.

[38] A. S. Kewitsch, T. W. Towe, G. J. Salamo, A. Yariv, M. Zhang, M. Segev, E. J. Sharp, R. R. Neurgaonkar, *Appl. Phys. Lett.* **1995**, *66*, 1865.

[39] A. Maimistov, A. Basharov, *Nonlinear Optical Waves*, Springer Science & Business Media, Berlin **2013**.

[40] V. Berger, *Phys. Rev. Lett.* **1998**, *81*, 4136.

[41] L. Simagina, E. Mishina, S. Semin, N. Ilyin, T. Volk, R. Gainutdinov, L. Ivleva, *J. Appl. Phys.* **2011**, *110*, 052015.

[42] J. J. Li, Z. Y. Li, D. Z. Zhang, *Phys. Rev. E* **2007**, *75*, 056606.

[43] A. Kumar, V. Kumar, B. Suthar, M. Ojha, K. S. Singh, S. Ojha, *IEEE Photonics Technol. Lett.* **2012**, *25*, 279.

[44] P. M. Johnson, A. F. Koenderink, W. L. Vos, *Phys. Rev. B* **2002**, *66*, 081102.

[45] X. Hu, P. Jiang, Q. Gong, *J. Opt. A: Pure Appl. Opt.* **2006**, *9*, 108.

[46] J. Martorell, R. Corbalan, *Opt. Commun.* **1994**, *108*, 319.

[47] H. Zhang, Q. Li, H. Zhu, L. Cai, H. Hu, *Opt. Mater. Express* **2022**, *12*, 2252.

[48] J. J. Li, Z. Y. Li, Y. Sheng, D. Z. Zhang, *Appl. Phys. Lett.* **2007**, *91*, 022903.

[49] S. Yamada, B. S. Song, S. Jeon, J. Upham, Y. Tanaka, T. Asano, S. Noda, *Opt. Lett.* **2014**, *39*, 1768.

[50] B. Omid, B. Abdolrahim, *Opt. Pura Apl.* **2020**, *53*, 9.